Acta Biomaterialia 169 (2023) 464–476

Contents lists available at ScienceDirect

Acta Biomaterialia

journal homepage: www.elsevier.com/locate/actbio

Full length article

Amyloidogenic propensity of self-assembling peptides and their adjuvant potential for use as DNA vaccines

Paresh C. Shrimali[a], Sheng Chen[b,1], Anirban Das[a,b,1], Rachel Dreher[b,1], Matthew K. Howard[b,1], Jeremy J. Ryan[b], Jeremy Buck[a], Darren Kim[a], Macy L. Sprunger[b], Jai S. Rudra[a,*], Meredith E. Jackrel[b,*]

[a] Department of Biomedical Engineering, Washington University, St. Louis, MO 63130, USA
[b] Department of Chemistry, Washington University, St. Louis, MO 63130, USA

ARTICLE INFO

Article history:
Received 23 January 2023
Revised 27 July 2023
Accepted 9 August 2023
Available online 14 August 2023

Keywords:
Amyloid
Immune response
Peptide nanofiber
Self-assembly
Vaccine
Yeast

ABSTRACT

De novo designed peptides that self-assemble into cross-β rich fibrillar biomaterials have been pursued as an innovative platform for the development of adjuvant- and inflammation-free vaccines. However, they share structural and morphological properties similar to amyloid species implicated in neurodegenerative diseases, which has been a long-standing concern for their successful translation. Here, we comprehensively characterize the amyloidogenic character of the amphipathic self-assembling cross-β peptide KFE_8, compared to pathological amyloid and amyloid-like proteins α-synuclein (α-syn) and TDP-43. Further, we developed plasmid-based DNA vaccines with the KFE_8 backbone serving as a scaffold for delivery of a GFP model antigen. We find that expression of tandem repeats of KFE_8 is non-toxic and efficiently cleared by autophagy. We also demonstrate that preformed KFE_8 fibrils do not cross-seed amyloid formation of α-syn in mammalian cells compared to α-syn preformed fibrils. In mice, vaccination with plasmids encoding the KFE_{32}-GFP fusion protein elicited robust immune responses, inducing production of significantly higher levels of anti-GFP antibodies compared to soluble GFP. Antigen-specific $CD8^+$T cells were also detected in the spleens of vaccinated mice and cytokine profiles from antigen recall assays indicate a balanced Th1/Th2 response. These findings illustrate that cross-β-rich peptide nanofibers have distinct physicochemical properties from those of pathological amyloidogenic proteins, and are an attractive platform for the development of DNA vaccines with self-adjuvanting properties and improved safety profiles.

Statement of significance

Biomaterials comprised of self-assembling peptides hold great promise for the development of new vaccines that do not require use of adjuvants. However, these materials have safety concerns, as they self-assemble into cross-β rich fibrils that are structurally similar to amyloid species implicated in disease. Here, we comprehensively study the properties of these biomaterials. We demonstrate that they have distinct properties from pathological proteins. They are non-toxic and do not trigger amyloidogenesis. Vaccination of these materials in mice elicited a robust immune response. Most excitingly, our work suggests that this platform could be used to develop DNA-based vaccines, which have few storage requirements. Further, due to their genetic encoding, longer sequences can be generated and the vaccines will be amenable to modification.

1. Introduction

Natural and *de novo* designed peptides that self-assemble into β-rich nanofibers have emerged as excellent building blocks for fabricating materials with a variety of biomedical applications [1].

* Corresponding authors.
E-mail addresses: srudra22@wustl.edu (J.S. Rudra), mjackrel@wustl.edu (M.E. Jackrel).
[1] These authors contributed equally to this work.

https://doi.org/10.1016/j.actbio.2023.08.015

Some of the simplest and most widely used synthetic peptides are amphipathic and comprised of alternating hydrophobic and polar/charged amino acids. Several such peptides have been shown to spontaneously associate to form fibrillar scaffolds in physiological buffers [1,2]. Self-assembling peptide biomaterials have several key advantages. First, they only require the synthesis of a simple peptide building block which then self-associates to form higher order complex structures. Additionally, functional groups can be appended to the peptides' *N*- or *C*-termini which are displayed in a multivalent fashion along the fibril surface, thereby imparting biofunctionality [3]. Numerous studies have demonstrated that self-assembling peptide biomaterials can support the growth of a variety of cell types and be used to deliver therapeutic drugs, exert antimicrobial effects, serve as theranostics, and act as immune adjuvants in vaccines [1,4,5].

A range of self-assembling peptide sequences have been designed that adopt a variety of secondary structures [6]. A particularly promising design is based on the cross-β structure where β-strands form the fibril axis which is stabilized by non-covalent interactions such as hydrophobic interactions, $\pi-\pi$ stacking, and electrostatic interactions [7]. While these cross-β rich scaffolds are highly promising as biomaterials, cross-β structures are also a defining characteristic of disease-relevant amyloid fibrils [8]. Indeed, accumulations of amyloid fibrils and pre-amyloid species are the pathological hallmark of many neurodegenerative disorders including Alzheimer's disease and related dementias, along with cardiac disorders, and diabetes [9–13]. Despite their structural and morphological similarity to disease-associated amyloids, β-rich fibrillar biomaterials have been explored for multiple biological applications, without reports of toxicity. We hypothesize that this is because the designed peptides aggregate extremely rapidly, and the pre-amyloid oligomeric species are likely the most toxic [14]. These differing kinetics likely bypass, or greatly decrease, the length of time that the nanofibers populate the highly toxic pre-amyloid oligomeric state. Another key feature of amyloids is their ability to seed further aggregation by nucleating amyloidogenesis [15]. Here, a small amount of amyloid fibrils can spontaneously enter cells and nucleate or 'seed' the amyloidogenesis of additional copies of the monomer, thereby rapidly increasing amyloidogenesis in neighboring cells [15,16]. It is crucial that any amyloid-inspired biomaterial be unable to seed the amyloid cascade of other amyloid-prone proteins. Therefore, it is important that the properties of cross β-sheet rich nanofibers be comprehensively characterized prior to their further application in these contexts [15,17].

The KFE sequence belongs to a class of amphipathic peptides with a $[XZXZ]_n$ pattern where X is a hydrophobic and Z is a charged or polar residue. KFE_8 (FKFEFKFE) is one of the best characterized sequences for use in the fabrication of hydrogel biomaterials. There are ample data pertaining to the effects of sequence length, pattern variation, and chiral substitutions on self-assembly and molecular packing of KFE_8 [7,18–21]. The two apolar faces of KFE_8 associate to form a cross-β motif that forms the backbone of the fibrils. We have demonstrated that KFE_8 is a powerful immune adjuvant for the development of vaccines and immunotherapies in multiple preclinical disease models [22–25]. To further apply KFE_8-based vaccines, it is crucial that they first be comprehensively characterized. Here, to accelerate translational efforts, different length repeats of KFE (KFE_8, KFE_{16}, and KFE_{32}), where KFE_{16} and KFE_{32} are comprised of 2 and 4 repeats of the KFE8 sequence, respectively, were expressed in a yeast model system and their toxicity and clearance mechanism was compared to that of the toxic amyloid-like protein TDP-43, which is implicated in amyotrophic lateral sclerosis (ALS) and frontotemporal dementia (FTD) [26]. We also investigated the seeding capacity of KFE_8 nanofibers because it is known that some proteins can cross-seed, whereby fibrils of one protein can trigger fibrillization of a different amyloid-prone protein [16]. Here, we tested the capacity of KFE_8 to cross-seed the aggregation of α-synuclein, a key protein implicated in Parkinson's disease (PD), using a mammalian biosensor cell line [27,28]. The successes we achieved in recapitulating the properties of the synthetic peptide nanofibers upon cellular expression suggest that this system might also be harnessed as a new form of DNA-based vaccine. Therefore, we generated lentivirus vectors expressing soluble GFP, α-syn-GFP or KFE_{32}-GFP for expression in mammalian cells, with GFP serving as both an expression marker and a model antigen. Mice were vaccinated with plasmids encoding soluble GFP, α-syn-GFP or KFE_{32}-GFP and antibody and cellular immune responses were evaluated. In comparison to prior studies where the toxicity testing was limited to cell viability assays, here we explore the safety profile of self-assembling peptides by directly comparing them to toxic amyloids in a range of cellular assays. Further, to our knowledge, this is the first report of DNA vaccines encoding self-assembling peptide sequences as adjuvants. Our results demonstrate that despite the structural and morphological similarity between pathological amyloids and self-assembling peptides, they have distinct immunological properties and safety profiles.

2. Materials and methods

2.1. Peptide synthesis

Peptides KFE_8 (≥90% purity) and KFE_{16} (~70% purity) were acquired from P3Bio and used without further purification. KFE_{32} was synthesized on a Liberty Blue microwave assisted peptide synthesizer (CEM) using standard Fmoc-SPPS chemistry on rink amide with DIC/Oxyma as coupling reagents and cleaved using a cocktail of trifluoroacetic acid (TFA), triisopropylsilane (TIS), and water (95:2.5:2.5). The crude peptide was pelleted using centrifugation, resuspended in cold diethyl ether, washed 5×, lyophilized, and stored at 4°C. Purification attempts were unsuccessful due to the intractable nature of KFE_{32}. Cy5-labeled KFE_8 was purchased from Genscript (90% purity). Co-assembled nanofibers were prepared for the seeding assay by mixing Cy5-KFE_8 and KFE_8 (1:9 mole ratio) followed by addition of water and vortexing to ensure complete mixing. This doping strategy has been previously reported for other self-assembling peptide systems and did not significantly impact fibril formation (**Fig. S7**).

2.2. Transmission electron microscopy

KFE_8 and KFE_{16} (0.25 mM in water) and KFE_{32} (0.0625 mM in water) were applied directly to glow discharged, 200 mesh, carbon-coated, copper grid (10 μL) for 2 min. Excess sample was blotted using filter paper. The grids were stained with uranyl acetate for 1 min and excess stain was removed using filter paper. Dark field and bright field images were taken with a JEOL JEM-2100 scanning transmission electron microscope (STEM) with an accelerating voltage of 120 kV.

2.3. Circular dichroism

CD spectra of the peptide solutions (same concentration as TEM above)) were recorded on a Jasco J-815 circular dichroism spectrometer. Spectra of the peptide solutions (3 scans) were collected at 20°C in a 1 mm quartz cuvette between 260 and 200 nm with a bandwidth of 1 nm, 0.1 nm step, and 2 s averaging time per step. Solvent background was subtracted.

2.4. Thioflavin-T (ThT) and ANS (8-anilino-1-napthalene sulfonic acid) assays

KFE_8 and KFE_{16} peptide fibrils, and KFE_{32} (50 μM in water) were mixed with ThT (50 μM in water) and fluorescence emis-

sion was measured (470–700 nm) upon excitation (440 nm) using a Synergy H1 microplate reader (BioTek). For ANS assays, peptide solutions (20 μM) were mixed with ANS (250 μM) and emission spectra was collected (380–700 nm) following excitation at 350 nm. ANS fluorescence spectra were also collected at varying peptide concentrations (10–50 μM). Intrinsic peptide fluorescence was measured and subtracted as background.

2.5. Yeast strains, media, and plasmids

All yeast were BY4741 or BY4741Δ*atg8*, acquired from the Yeast Knockout Collection [29]. pAG423GAL-ccdB-eGFP plasmid for yeast expression was obtained from Addgene [30]. Strains expressing TDP-43 and α-syn have been described previously [31]. Yeast were grown in rich medium (YPD) or in synthetic media lacking the appropriate amino acids. Media was supplemented with 2% glucose, raffinose, or galactose. To construct KFE_8 plasmids, repeating sequences of KFE_8 interspersed with flexible glycine-serine linker regions were synthesized by IDT with flanking Gateway cloning sites. KFE_{16} and KFE_{32} refer to 2x and 4x repeats of this KFE_8 sequence. These fragments were then inserted into pAG423GAL-ccdB-eGFP [30] by Gateway cloning to generate KFE_8 tagged with GFP at the C-terminus. Final sequences were: KFE_8: MFKFEFKFEGSGSGSGS-(eGFP), KFE_{16}: MFKFEFKFEGSGSGSGSFKFEFKFEGSGSGSGS-(eGFP), and KFE_{32}: MFKFEFKFESGSGSGSGFKFEFKFEGSGSGSGSGFKFEFK FEGGSGSGSGFKFEFKFEGSGSGSGS-(eGFP).

2.6. Yeast transformation and spotting assays

Yeast were transformed according to standard protocols using polyethylene glycol and lithium acetate [32]. For the spotting assays, yeast were grown to saturation overnight in raffinose supplemented dropout media at 30°C, normalized to A_{600nm} = 1.5, serially diluted, and spotted in duplicate onto synthetic dropout media containing glucose or galactose. Plates were analyzed after growth for 2-3 days at 30°C. Each experiment was repeated three times.

2.7. Immunoblotting and microscopy

Yeast were grown and induced in galactose containing medium for 5 h from overnight cultures supplemented with raffinose. Cultures were normalized to A_{600nm} = 0.6, 8 mL cells were harvested, treated in 0.1M NaOH for 5 min at room temperature, and cell pellets were then resuspended into 1x SDS sample buffer and boiled for 4 min. Lysates were cleared by centrifugation at 14,000 rpm for 2 min and then separated by SDS-PAGE (4–20% gradient, BioRad), and transferred to a PVDF membrane. Membranes were blocked in Odyssey Blocking Buffer (LI-COR). Primary antibody incubations were performed at 4°C overnight. Antibodies used: anti-GFP monoclonal (Roche Applied Science), anti-TDP-43 polyclonal (Proteintech), and anti-PGK monoclonal (Invitrogen). Membranes were imaged using a LI-COR Odyssey FC Imaging system. For microscopy, strains were grown as for immunoblotting. After 15 h induction at 30°C, cultures were harvested and processed for microscopy. All imaging was performed using live cells treated with Hoechst dye. Yeast images were collected at 90x magnification on a Nikon Eclipse Te2000-E microscope and processed using ImageJ software. All experiments were repeated at least three times, and representative images are shown.

2.8. Filter retention assays

Yeast were grown and induced as for immunoblotting. Following induction, cultures were normalized to A_{600nm} = 0.5, and 5 mL of cells were collected and washed with sterile water. Cells were resuspended in 500 μL spheroplasting solution (1.2 M D-sorbitol, 0.5 mM $MgCl_2$, 20 mM Tris, 50 mM β−mercaptoethanol, 0.5 mg/mL Zymolyase 100T, pH 7.5) for 1 h at 30°C with light shaking. Spheroplasts were pelleted by centrifugation at 500x RCF for 5 min, and supernatant was discarded. Samples were then resuspended in 100 μL lysis buffer (100 mM Tris, pH 7.5, 500 mM NaCl, 5 mM $MgCl_2$, 10 mM β-mercaptoethanol, 0.5% Triton, and 1% yeast Protease Inhibitor cocktail). Samples were vortexed at high speed for 1 min and then incubated at room temperature for 10 min. Cells were then flash frozen in nitrogen, thawed at room temperature, and boiled for 5 min where indicated. 33 μL of sample buffer (2X TAE, 20% glycerol, 10% β−mercaptoethanol, and 0.0025% bromophenol blue) was added, followed by incubation for 5 min at room temperature. 15 μL of each extract was applied to a nonbinding cellulose acetate membrane using a Minifold I 96-well spot-blot array system (GE). The membrane was then washed with PBST and the remaining sample was diluted in PBST (3 sample:1 PBST) and 5 μL was applied onto a nitrocellulose membrane. After both membranes were allowed to dry, they were then re-wetted in PBST for 10 min. Membranes were blocked and imaged as described for immunoblotting. Bound protein was quantified using ImageStudio Lite software (LICOR). The reported CA/NC ratio is the ratio of signal on the cellulose acetate (CA) and nitrocellulose (NC) membrane. Values were normalized to a vector control run in parallel.

2.9. Preparation of α-synuclein PFFs

Plasmid for expression of α-synuclein was from Peter Lansbury [33]. α-Synuclein was expressed in *E. coli* BL21-DE3-RIL cells (Invitrogen), where expression was induced at OD_{600} = 0.6 with 1 mM IPTG for 2 h at 37°C. Cell pellets were resuspended in osmotic shock buffer (30 mM Tris, pH 7.2, 2 mM EDTA, 40% sucrose) and incubated for 10 min at room temperature with vortexing. The lysate was then cleared by centrifugation. Nucleic acids were then removed by streptomycin sulfate precipitation (10 mg/mL final concentration) and cleared by centrifugation. The supernatant was then boiled for 10 min and the soluble protein was loaded on to a bed of DEAE sepharose beads for anion-exchange batch purification. The beads were washed with wash buffer (20 mM Tris, pH 8.0, 1 mM EDTA) and then eluted with elution buffer (20 mM Tris, pH 8.0, 300 mM NaCl, 1mM EDTA). The eluted protein was then dialyzed against α-syn fibrillization buffer (20 mM Tris-HCl, pH 8.0, 100 mM NaCl). Endotoxin was removed using a High-Capacity Endotoxin Removal Spin Column (Pierce) and confirmed using a Charles River Endosafe Cartridge. The protein was then flash frozen and stored at -80°C until use.

To prepare α-syn PFFs, monomer was thawed and passed through a 0.2 μm syringe filter. The protein was then diluted to 5 mg/mL in fibrillization buffer and incubated at 37°C with agitation at 1,500 rpm in an Eppendorf Thermomixer for 7 days. The resulting mixture was centrifuged at 15,000 rpm for 30 min at room temperature. The supernatant was then removed and fibrils were resuspended to achieve 5 mg/mL fibrils, as measured by a BCA assay. Fibrils were then flash frozen and stored at -80°C until use.

To prepare labeled α-syn, 5 mg/mL monomeric α-syn was filtered through a 0.2 μm syringe filter and diluted to 2 mg/mL in 0.1 M $NaHCO_3$. Alexa Fluor 568 NHS Ester (A20003) was dissolved in DMSO to 10 mg/mL. Alexa dye was added in 2.1:1 molar ratio of dye:α-syn and mixed by stirring at room temperature for 1 h. Unbound dye was removed using Bio-Spin P-6 Gel Columns (Bio-Rad #7326227). The Alexa-568 labeled α-syn was aliquoted, flash frozen, and stored at -80°C. To prepare labeled α-syn PFFs, both monomeric Alexa-568 labeled α-syn and unlabeled α-syn were filtered through a 0.2 μm syringe filter. Alexa-568-α-Syn was mixed with unlabeled α-syn (5% labeled) in 40 mM HEPES pH 7.4,

150 mM KCl, and 20 mM $MgCl_2$. The mixture was then incubated at 37°C with agitation at 1,500 rpm in an Eppendorf ThermoMixer with ThermoTop for 7 days to produce mature fibrils. The resulting mixture was centrifuged at 15,000 rpm for 30 min at room temperature. The supernatant was then removed and PFFs were resuspended in 20 mM Tris pH 8, 100 mM NaCl to achieve 5 mg/mL fibrils. Protein was then aliquoted, flash frozen and stored at -80°C until use.

2.10. HEK293T cell culture and FRET biosensor cell assays

HEK293T biosensor cells (HEK293T-α-syn-CFP/α-syn-YFP) were obtained from David Holtzman [28]. Cells were grown in Dulbecco's modified high glucose Eagle's medium (DMEM) supplemented with 10% fetal bovine serum (FBS), and 1% penicillin/streptomycin. For FRET seeding assays, the biosensor cells were plated in 96-well plates at a density of 35 K cells per well. 24 h following plating, PFFs were applied. Here, α-syn or Cy5-KFE_8 fibrils were diluted in fibrillization buffer to the appropriate concentration and sonicated in a cup horn water bath sonicator for 3 min. The fibrils were then mixed with Lipofectamine 3000 (Invitrogen) at 0.5 μL Lipofectamine per well, incubated for 10 min at room temperature, and applied to the biosensor cells. After 48 h, cells were trypsinized, transferred to a 96-well plate, and fixed with 4% paraformaldehyde for 15 min at 4°C in the dark. Cells were then resuspended in 150 μL chilled MACSQuant Flow Running buffer for analysis in a MACSQuant VYB flow cytometer. Fluorescence was measured using settings for CFP (ex: 405 nm, em: 450 nm, bw: 50 nm), YFP (ex: 488 nm, em: 525 nm, bw: 50 nm), FRET (ex: 405 nm, em: 525 nm, bw: 50 nm), and Cy5 (ex: 561 nm, em: 661, bw: 20 nm). Fluorescence compensation was performed with control cell lines each time prior to sample analysis. FRET signal was used to distinguish cells with α-syn aggregation from cells without α-syn aggregation. Integrated FRET density was calculated by multiplying the percent cells with FRET signal by median FRET intensity of the FRET-positive cells. To quantify KFE_8 fibril internalization, a bivariate plot of Cy5 vs CFP was created to introduce a polygon gate to exclude all of the Cy5-negative cells treated with only lipofectamine/buffer and to include the Cy5-positive cells treated with KFE_8 fibrils. The quantification for KFE_8 internalization was based on percent Cy5-positive cells. All data analysis was performed with FlowJo V10 software. Images were collected at 20x magnification on a Nikon Eclipse Te2000-E microscope and processed using ImageJ software.

2.11. Generation of lentiviral plasmids

293LTV cells were kind gift from Dr. Kian Lim, Washington University in St. Louis. A20 cells were kind gift from Dr. John F. DiPersio, Washington University in St. Louis [34]. pLenti CMV GFP Puro (658-5) was a gift from Eric Campeau & Paul Kaufman (RRID:Addgene_17448) [35]. Packaging pMDLg/pRRE (Addgene plasmid #12251), envelope pMD2.G (Addgene plasmid #12259), and regulatory plasmids pRSV-Rev (Addgene plasmid # 12253) were a gift from Didier Trono [36]. The $\propto$-synuclein tagged GFP or $KFE8_{32}$ tagged GFP constructs were derived by sub-cloning services from Genescript USA Inc., into pLenti backbone by replacing GFP with α-Syn-GFP or KFE_{32}-GFP.

2.12. Animals and immunization

All experimental procedures were approved by the Institutional Animal Care and Use Committee of Washington University in St. Louis. 20 µg (100 µL of PBS) of pLenti-GFP or α-Syn-GFP or KFE_{32}-GFP plasmids were injected intramuscularly into 6-8 wk old female BALBC mice three times with 14 days between immunizations. Blood was drawn 10 days after the last dose and sera was collected for ELISA. Spleens were harvested and splenocyte cultures were prepared according to published protocols and stained with T-select H-2Kd restricted $GFP_{200\text{-}208}$ tetramer (MBL Bio #TS-M525-1) to assess cellular immune responses. Splenocytes (10^6/well) were also stimulated *in vitro* with GFP (2 μg/ml) for 5 days and the supernatant collected for analysis of cytokines.

2.13. Antibody titers and isotyping

High binding ELISA plates (Corning #3361) were coated with 1 μg/mL GFP in PBS and incubated overnight at 4°C. The wells were blocked for 1 h at RT with 1% BSA in PBST buffer (PBS with 0.05% Tween20, 100 μL/well). Serial dilutions of the sera were prepared in the blocking buffer and added to the wells (100 μL/well for 1 h at RT) followed by secondary HRP-conjugated goat anti-mouse IgG (1:5000, 100 μL/well) for 30 min. For isotyping, HRP-conjugated secondary isotypes (IgG1, IgG2b, IgG2c, IgG3, IgM, or IgE; Southern Biotech) were added (1:4000, 100 μL/well for 1 h at RT) after serum dilutions prior to development. Plates were washed 3-5 times between each coating step. The assay was developed using TMB solution (100 μL/well) for 15 min and the reaction was quenched with 1 M phosphoric acid (100 μL/well). Absorbance was recorded at 450 nm using a Biotek Synergy microplate reader and background absorbance from non-antigen coated wells was subtracted.

2.14. Cellular immune responses

Induction of GFP-specific T cell response was quantified by measuring the tetramer positive $CD8^+$T cells in spleen of vaccinated mice via flow cytometry. Briefly, splenocytes from vaccinated mice were prepared following RBC lysis of whole spleen suspensions as reported previously. Cells were stained with Zombie NIR fixable viability dye (Biorad #423105) for 15 min, washed in once with FACS buffer, and stained with T-select H-2Kd restricted $GFP_{200\text{-}208}$ (HYLSTQSAL) tetramer (PE, # TS-M525-I, MBL Inc.) followed by CD3-PE-Cy7 (Biolegend #100220) and CD8-APC (eBioscience #17-0081-82) staining. Total 10^6 events were recorded on NovoCyte instrument (ACEA Biosciences, USA.) and the data were analyzed by FlowJo v.10 software (FlowJo, LLC). To assess cytokine production, splenocytes (10^6/well) were plated in 24-well plates and treated with GFP (2 μg/ml for 5 days or with PBS as control). Supernatant was collected and cytokines were quantified using mouse cytokine & chemokine convenience 6-Plex kit (IL-2, IL-4, IL-5, IL-10, IFN-γ and TNF-α; # LXSAMSM-06, R&D systems) using Luminex xMAP according to manufacturers protocols.

2.15. Statistical analysis

All quantitative results were obtained from three or more samples per group. To ensure reproducibility and rigor, two independent animal studies (4-5 mice per group) were conducted and cumulative antibody levels tetramer-positive $CD8^{\pm}$T cell frequency are shown. Data are expressed as mean±S.E. and statistical analysis was performed using a one-way or two-way ANOVA with Tukey/Sidak's/Dunnett's multiple comparison test. $^*p \leq 0.05$, $^{**}p \leq 0.01$, $^{***}p \leq 0.001$, $^{****}p \leq 0.0001$.

3. Results

3.1. Testing the toxicity and clearance mechanism of KFE repeat constructs in yeast

Saccharomyces cerevisiae, Baker's yeast, has long been a useful model system for studying biology. Though simple, yeast is highly

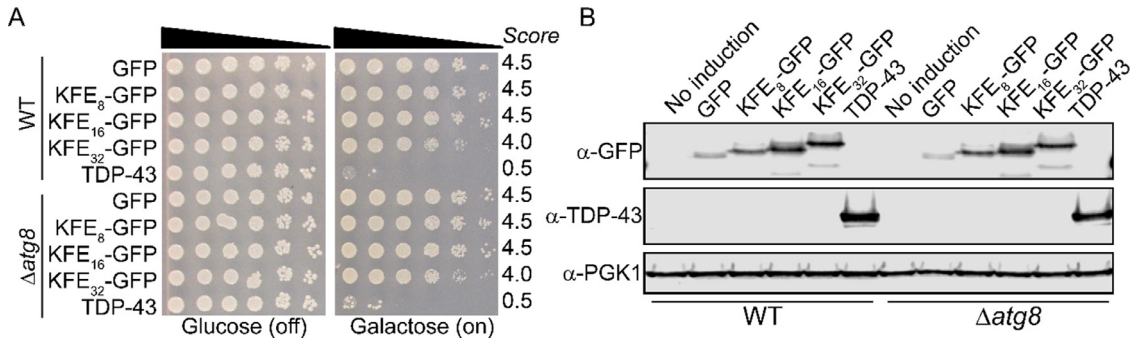

Fig. 1. KFE_8-GFP fusions are nontoxic in yeast. (A) BY 4741 and BY 4741 Δ*atg8* yeast was transformed with galactose-inducible KFE_8-GFP fusions of varying lengths along with a GFP and TDP-43 control. The strains were serially diluted 5-fold and spotted onto glucose (off) or galactose (on) media. Toxicity was scored on a scale from 0 to 6 based on the average number of spots from four replicates. (B) Strains from (A) were induced for 5 h, lysed, and immunoblotted. PGK1 serves as a loading control.

genetically tractable, and genetic pathways are highly conserved between yeast and humans [37]. Yeast has been shown to be an excellent model system for studying complex human diseases including ALS/FTD, Parkinson's disease, Alzheimer's disease, diabetes, and sarcoma [38–45]. We therefore sought to study the properties of the repeat peptide constructs in yeast, compare their properties to those of disease-associated amyloid and amyloid-like proteins, and follow their mechanism of clearance. To test the effects of intracellular expression of the constructs, we generated plasmids encoding 1, 2, or 4 repeats of the sequence FKFEFKFE for expression in yeast. Each repeat was separated by a flexible glycine-serine linker, and to monitor expression and localization, we fused each construct to eGFP. We used the 423GAL plasmid to drive galactose-inducible expression of the genes, and we expressed KFE_8, KFE_{16}, and KFE_{32}, along with a GFP control. We also included the amyloid-like protein TDP-43, which has been implicated in ALS/FTD and has been shown to be highly toxic and aggregate in yeast [46]. As expected, TDP-43 was highly toxic in yeast, while KFE_8 and KFE_{16} were nontoxic. KFE_{32} was just slightly toxic (Fig. 1A). Expression of each of the constructs was confirmed via immunoblotting, and we also observed the expected increase in molecular weight corresponding to increased number of repeats (Fig. 1B).

It has been demonstrated that these peptide nanofibers engage the autophagy machinery in mammalian cells [47]. Such off-target effects could prove problematic for ultimate therapeutic applications of the nanofibers, particularly in elderly populations known to have impaired autophagy, though toxicity of the nanofibers has not been noted in mammalian cell studies. Therefore to validate our yeast model, we sought to assess if these proteins also engage autophagy in yeast. We assessed the toxicity of each of the fusions in Δ*atg8* yeast and found that toxicity was not modified in this background as compared to WT yeast (Fig. 1A). We therefore conclude that the repeat peptide constructs are not toxic and toxicity is not exacerbated under autophagy-deficient conditions.

3.2. KFE repeat peptides form insoluble inclusions in yeast

Amyloid proteins are known to form insoluble inclusions that are resistant to boiling and other denaturing conditions. To determine if the KFE repeats formed insoluble species in yeast, we employed a filter retention assay [48]. Here, following induction of expression as for immunoblotting, extracts are applied to a nonbinding cellulose acetate and a binding nitrocellulose membrane in parallel. Larger insoluble species will be retained on the cellulose acetate membrane while smaller species will pass through the membrane. Proteins that form highly stable amyloid conformers will be resistant to high concentrations of denaturant and boiling. Here, we found that each of the KFE_8 fusions strongly bound

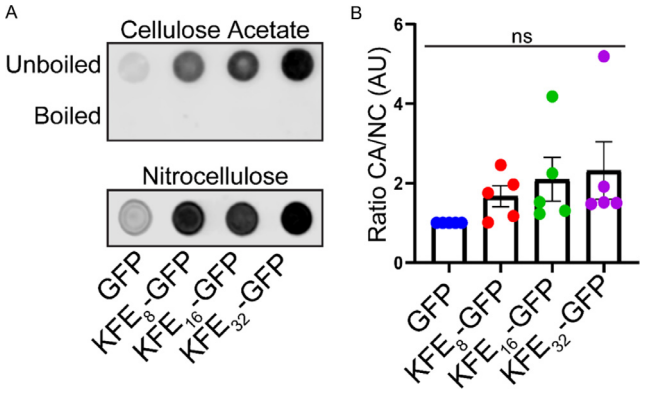

Fig. 2. KFE-GFP fusions are insoluble in yeast. (A) Filter retention assays of the three KFE-GFP fusions expressed in WT yeast. Cells were induced for 5 h, lysed, and passed in duplicate through a nonbinding cellulose acetate membrane and a binding nitrocellulose control membrane. Samples were also boiled and passed through the cellulose acetate membrane. Peptides were then detected by immunoblotting for the GFP epitope. Experiments were performed in triplicate with independent transformations, representative results are shown. (B) The ratio of binding to the cellulose acetate (CA) to nitrocellulose (NC) membrane for the unboiled samples was quantified and normalized to the vector control. Dots show biological replicates, bars show means, and error bars show SEM ($N = 5$). A one-way ANOVA with Tukey's multiple comparison test was used to assess differences among each of the strains and no significance was found.

to the cellulose acetate membrane as compared to the GFP control (Fig. 2A). As controls, we also included yeast expressing α-syn and a polyglutamine expansion (**Fig. S1**). Following boiling, none of the samples were retained on the cellulose acetate membrane, with the exception of α-syn and polyglutamine. The ratio of material retained on the two membranes was quantified and we observed a predicted increase in retention on the cellulose acetate membrane that correlates with increased length of the construct (Fig. 2B). We therefore conclude that the repeat peptide constructs assemble into stable, insoluble species, but that these species are not as stable as amyloid species and can be disrupted at high temperatures. We also aimed to purify these KFE-GFP constructs to confirm that GFP does not perturb fibrillization and that the materials form nanofibrils in yeast. However, we found that the KFE repeat sequence drives the construct to accumulate in inclusion bodies, and purification was not possible in either the native or denatured state (**Fig. S2**).

3.3. KFE repeat peptides form foci in yeast that are cleared by autophagy

We next sought to visualize the properties of the KFE repeat peptides in yeast using fluorescence microscopy. We studied each

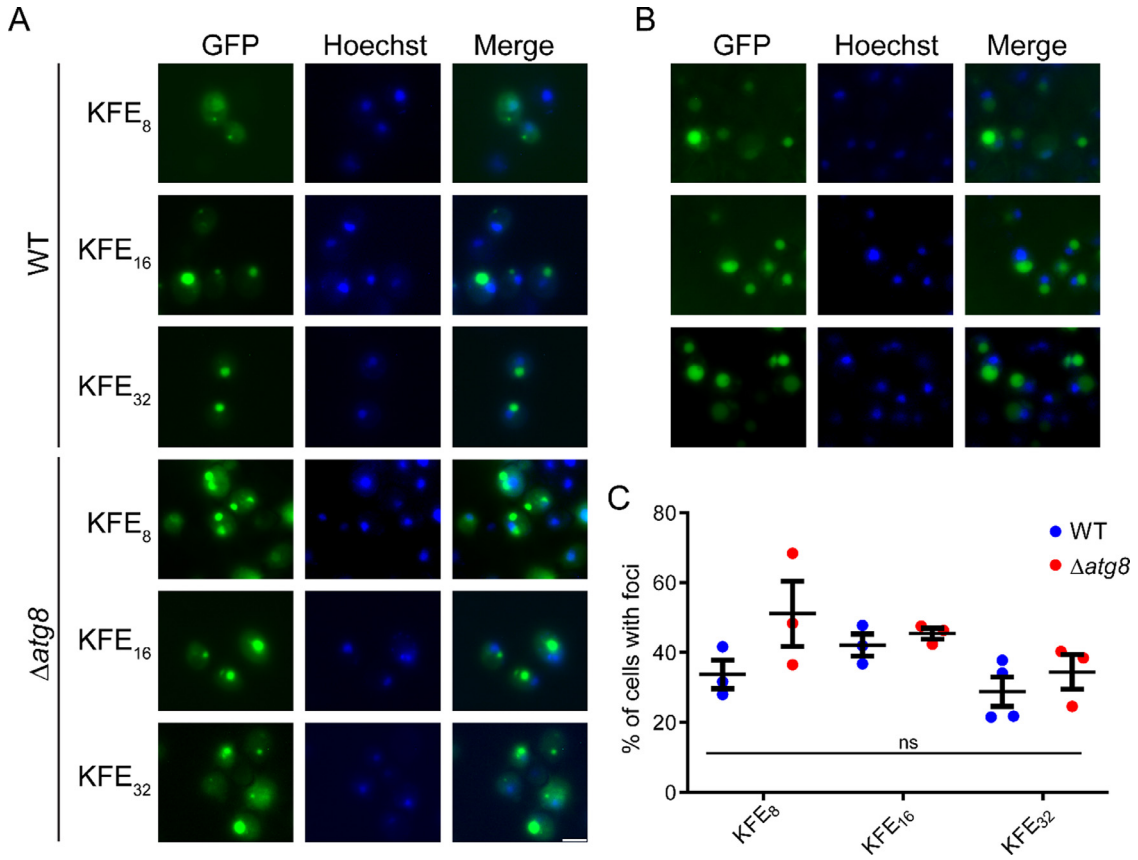

Fig. 3. KFE-GFP fusions form foci in yeast. (A) Fluorescence microscopy of the three KFE-GFP fusions expressed in WT and Δ*atg8* yeast. Strains were induced for 15 h, stained with Hoechst dye to visualize nuclei (blue), and imaged. Foci formed in each strain, with no clear differences among the strains. Representative images are shown, scale bar = 5 μm, all images are at the same scale. (B) Additional images of strains shown in (A). In some cells in the WT background, vacuolar accumulation of GFP was observed. No vacuolar accumulation of GFP was observed for cells in the Δ*atg8* background. (C) Quantification of microscopy experiments shown in (A). Error bars show SEM. A one-way ANOVA with Tukey's multiple comparison test was used to assess differences among each of the strains and no significant differences were found. (For interpretation of the references to colour in this figure legend, the reader is referred to the web version of this article.)

of the strains and found that expression of each of the six strains elicited formation of foci, or areas of punctate fluorescence, in yeast (Fig. 3A). We quantified these effects and found no significant differences in the number of cells harboring foci that correlated with length of the KFE_8 repeat, although the foci did appear larger in strains expressing KFE_{16} and KFE_{32} as compared to KFE_8. We also observed that many cells in the WT background displayed GFP fluorescence in the vacuole (Fig. 3B), while vacuolar accumulation was not observed in the Δ*atg8* background. We quantified these effects and saw a subtle, but consistent, increase in the number of cells with foci in the Δ*atg8* background as compared to the WT background (Fig. 3C). These shifts in localization appear to happen without any substantial changes in expression level between the WT and Δ*atg8* strains. Based on this increased number of foci in the autophagy-deficient strain, and the accumulation of vacuolar KFE, we conclude that they are trafficked through the autophagy pathway in yeast, as they are in mammalian cells, yet this does not trigger toxicity.

3.4. Self-assembly of KFE variants

We next generated these synthetic peptides to characterize their solubility and for use in subsequent seeding assays. Scanning transmission electron microscope (STEM) images indicated that KFE_8 and KFE_{16} assemble into high aspect ratio nanofibers as expected, whereas KFE_{32} assembled into amorphous aggregates, likely due to challenges with synthesis and purification of such long repeat peptides (**Fig. S3**). Circular dichroism (CD) spectroscopy showed that KFE_8 assembled into the expected cross-β structure (minima at ~204 nm and ~214 nm) whereas the secondary structure of KFE_{16} was indicative of a classical β-sheet (minima at 215–220 nm) which is in agreement with other amphipathic 16-mer sequences such as EAK16 and RADA16 [49] (**Fig. S4**). We used ThT fluorescence to assess the β-rich content of KFE assemblies and data indicated enhanced fluoresence with increasing length (**Fig. S5**). In contrast to ThT that incorporates into the grooves along the long axis of the fibril, ANS binds to exposed hydrophobic patches as well as integrates into hydrophobic cavities and our data indicated enhanced ANS fluorescence emission with increasing repeat length (**Fig. S6**). Together, these data suggest that KFE8 and KFE16 undergo self-assembly into supramolecular β-rich architectures whereas KFE32 forms amorphous aggregates.

3.5. Peptide nanofibers cannot cross-seed aggregation of α-synuclein

Amyloid fibrils are known to spontaneously enter cells and seed aggregation of other copies of monomeric protein. These features underpin the cell-to-cell transmissibility and infectious nature of amyloid, allowing for a small quantity of seed to rapidly accelerate conversion of monomer to adopt the amyloid fibril conformation [50]. Further, cross-seeding is a phenomenon by which amyloid fibrils comprised of one protein can nucleate amyloid formation by a protein of a different sequence. Given the resemblance of the secondary structure of KFE nanofibers to disease-associated amyloid and amyloid-like proteins, it is of crucial importance that the KFE nanofibers be incapable of seeding aggre-

gation of disease-associated amyloid proteins. To test this idea, we employed HEK293T α-synuclein biosensor cells [27,28]. Here, one copy of α-synuclein is fused to cyan fluorescent protein (CFP) while another copy is fused to yellow fluorescent protein (YFP). CFP and YFP function as a pair of fluorophores that can readily undergo fluorescence resonance energy transfer (FRET) when in close proximity, such as upon aggregation. As previously shown, when pre-formed α-synuclein fibrils (PFFs) are added to cell culture medium, the PFFs are internalized by the HEK cells and trigger aggregation of α-synuclein which is quantified by measuring the FRET signal by flow cytometry [28].

To test if the KFE nanofibers can seed α-synuclein biosensor cells, we first confirmed uptake of the fibrils by flow cytometry using Cy5 labeled KFE fibrils. Internalization of the nanofibers was robust, with approximately 10% of cells displaying a Cy5 positive signal on addition of 100 nM fibrils. When the concentration was increased to 200 nM, nearly 40% of cells were Cy5 positive (Figs. 4A, S8A). We next compared internalization of KFE fibrils to α-syn monomer and α-syn PFFs using fluorescently labeled proteins (Figs. 4B, S8B). We find that α-syn monomer is most readily internalized, with approximately 70% of cells showing internalized α-syn. α-Syn PFFs are taken up less readily, with approximately 50% of cells showing internalized PFFs. Approximately 30% of cells take up labeled KFE_8 fibrils, indicating that the KFE_8 fibrils are internalized more similarly to amyloid fibrils than monomeric protein. We then applied the proteins to assess seeding. Here, application of just 50 nM α-syn PFFs is sufficient to trigger a robust FRET signal (Figs. 4C, S8C), with over 25% of cells displaying FRET. When Cy5-KFE_8 preformed fibrils are applied instead of α-syn PFFs we observe no increase in FRET (Fig. 4D). We increased the concentration of Cy5-KFE_8 to as high as 200 nM and still observed no FRET signal (Fig. 4D), confirming that the nanofibers do not seed α-synuclein aggregation. We also applied 10 μM KFE_8 nanofibers without the Cy5 tag to ensure there was no interference of the tag with the FRET pair and still observed no seeding. We also directly compared application of KFE_8, α-syn monomer, and α-syn PFFs all harboring the fluorescent tag and observe similar results (Figs. 4E, S8D). To further corroborate these results, we imaged these cells using fluorescence microscopy. Again we observe an abundance of foci upon application of α-syn PFFs, while no foci are observed upon application of the KFE_8 nanofibers (Fig. 4F-H). Thus we conclude that the KFE nanofibers can enter cells similarly to amyloid fibrils, but they cannot cross-seed α-syn. Prior studies by Zottig et al. also demonstrated that a 10-mer peptide (SNNFGAILSS) derived from the amyloidogenic segment of the islet amyloid polypeptide is capable of self-assembling into nanofibers but not seeding amyloid formation [51].

3.6. Vaccination with plasmids encoding KFE_{32}-GFP elicits a robust antibody response

Armed with our characterization data, we next tested the immunogenicity of plasmid vaccines containing KFE_{32} tagged with GFP as our model antigen. The reason for this choice is because our ultimate goal is to express longer epitopes via plasmid delivery, and these additional repeats can be easily generated through plasmid vaccination. Further, prior studies reporting on plasmid vaccines composed of poly-Q tails attached to GFP have reported a length-dependent increase in immunogenicity [52]. Thus, we chose to conduct our immunological studies using the longest repeat KFE_{32}-GFP construct. DNA-based vaccines have many advantageous features as compared to synthetic peptide vaccine strategies such as decreased cost, improved stability, and the ability to construct longer sequences than can be accomplished using solid-phase peptide synthesis. In our studies, we encountered significant barriers in the synthesis and purification of KFE_{32} (**Figs. S3-7**) and there is no precedence in the literature for solid phase synthesis of amphipathic peptides beyond 16 residues. This provides a strong rationale for delivering the constructs as DNA vaccines. However, synthesis in the host may also lead to different assembly patterns and architectures than when synthesized *in vitro*. Here, we primed and boosted groups of Balb/c mice with plasmids encoding GFP, α-syn-GFP or KFE_{32}-GFP and assayed the levels of anti-GFP antibodies in the sera. Data indicated that mice vaccinated with the KFE_{32}-GFP or α-syn-GFP construct produced significantly higher levels of anti-GFP antibodies as compared to soluble GFP at the highest dilution tested. (Fig. 5A). This difference can be ascribed to the monomeric or oligomeric nature of soluble GFP or α-syn-GFP and KFE_{32}-GFP respectively which could potentially fibrillize *in vivo* to form higher molecular weight, high aspect ratio nanofibrils that mimic danger signals and activate the immune system. In a series of serum dilutions, higher absorbance values were detected in mice receiving the α-syn or KFE_{32} tagged GFP compared to the soluble form. To determine the nature of the antibody response, isotypes IgG1, IgG2a, IgG2b, and IgG2c, IgG3, IgM, and IgE were assessed using ELISA. Data indicated detectable levels of IgG1, IgG2a, IgG2b and IgM (**Fig. S9**). These findings are exciting as they demonstrate that these vaccines can be produced upon expression driven by a plasmid in a host. This will allow for more antigenic complexity in the construction of such vaccines than is possible with *in vitro* synthesis.

3.7. Vaccination with plasmids encoding KFE_{32}-GFP elicits a robust T cell response

Immunization with DNA is known to be an effective inducer of cellular immunity. Having demonstrated that our constructs elicit a robust antibody response, we next sought to evaluate the ability of GFP, α-syn-GFP or KFE_{32}-GFP constructs to potentiate the production of antigen-specific $CD8^+$T cells. Spleens from vaccinated mice were used in antigen recall assays and the frequency of tetramer-postitive $CD8^+$T cells was quantified using flow cytometry. Production of antigen-specific cells were detected in mice receiving all constructs without measurable statistical differences (Figs. 5, S10). Importantly, both α-syn and KFE_{32} fusion constructs were found to elicit equivalent levels of antigen-specific $CD8^+$T cells. The augmentation of antibody responses, isotype class-switching, and tetramer+ $CD8^+$T cells also point to the possibility that KFE_{32}-GFP could efficiently trigger $CD4^+$T cell mediated helper immunity. To investigate the involvement of T cell help, splenocytes from immunized mice were stimulated *in vitro* with soluble GFP (cognate antigen), and the production of interferon-γ (IFN-γ), tumor necrosis factor-α (TNF- α), interleukin-2 (IL-2), interleukin-4 (IL-4), interleukin-5 (IL-5), and interleukin-10 (IL-10) was measured using a multiplex assay. These cytokines were selected to provide measures of either a Th1 response (IFN-γ, TNF- α, and IL-2) or a Th2 response (IL-4, IL-5, IL-10). Data indicated significantly higher production of all cytokines in splenocyte cultures of mice vaccinated with soluble GFP, α-syn-GFP, or KFE_{32}-GFP constructs compared to controls (splenocytes from the same mice that did not receive the cognate GFP stimulus) (Fig. 6). The production of classical cytokines associated with both Th1 and Th2 phenotypic T cells suggests a balanced immune response.

4. Discussion

A crucial challenge in vaccine development is to achieve a balance between immunogenicity and safety [53]. Most of the currently used vaccines rely on co-administration of antigens with adjuvants to enhance, maintain, and direct the adaptive immune response. In the U.S., only handful of adjuvants (alum, AS04, and CpG) are currently licensed for human use [54,55], though a new

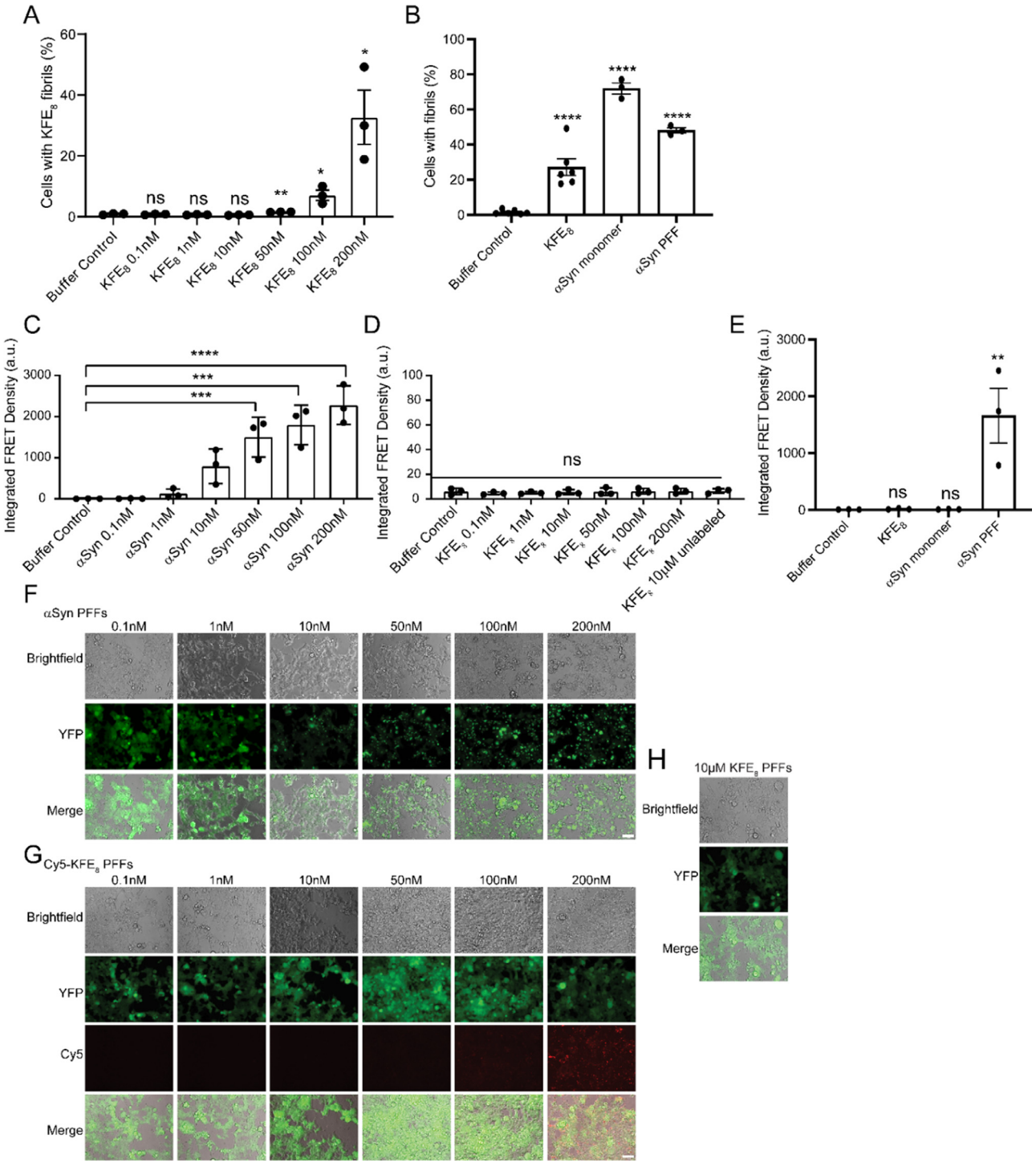

Fig. 4. KFE_8 nanofibers are internalized by HEK biosensor cells and do not cross-seed α-synuclein. (A) Cy5-KFE_8 nanofibers were applied to HEK biosensor cells and internalization was monitored by flow cytometry. Quantification is based on Cy5 signal. Values were compared to buffer control using a series of two-tailed t-tests ($N = 3$, biological replicates are shown as dots, bars represent means ± SEM, $^{*}p \leq 0.05$, $^{**}p \leq 0.01$). (B) Cy5-KFE_8 nanofibers, Alexa568-α-syn monomer, or Alexa568-α-syn PFFs were applied to HEK biosensor cells and internalization was monitored by flow cytometry. Quantification of cells with fibrils is based on Cy5 or Alexa 568 signal, respectively. Values were compared to buffer control using a series of two-tailed t-tests ($N \geq 3$, biological replicates are shown as dots, bars represent means ± SEM, $^{****}p \leq 0.0001$). (C) HEK α-synuclein biosensor cells were seeded with α-syn PFFs at the indicated concentrations. Seeding of α-syn was monitored by flow cytometry. Integrated FRET density for the α-syn PFFs were quantified from the experiments. (D) Experiments were performed as in C, but using KFE_8 PFFs at the indicated concentrations. Values in C and D are compared to buffer treatment using a one-way ANOVA with a Dunnett's multiple comparisons test ($N = 3$, biological replicates are shown as dots, bars represent means ± SEM, $^{***}p \leq 0.001$, $^{****}p \leq 0.0001$). (E) Labeled materials as tested for internalization in B were applied to HEK α-synuclein biosensor cells and seeding was monitored as in D. (F) α-Syn PFFs were added to biosensor cells at the indicated concentration and imaged. (G) Experiments were performed as in F but with Cy5-KFE_8 PFFs instead of α-syn. (H) Experiments were performed as in G but with unlabeled KFE_8 at higher concentration. Scale bar = 20 μm, scaling is the same in all images.

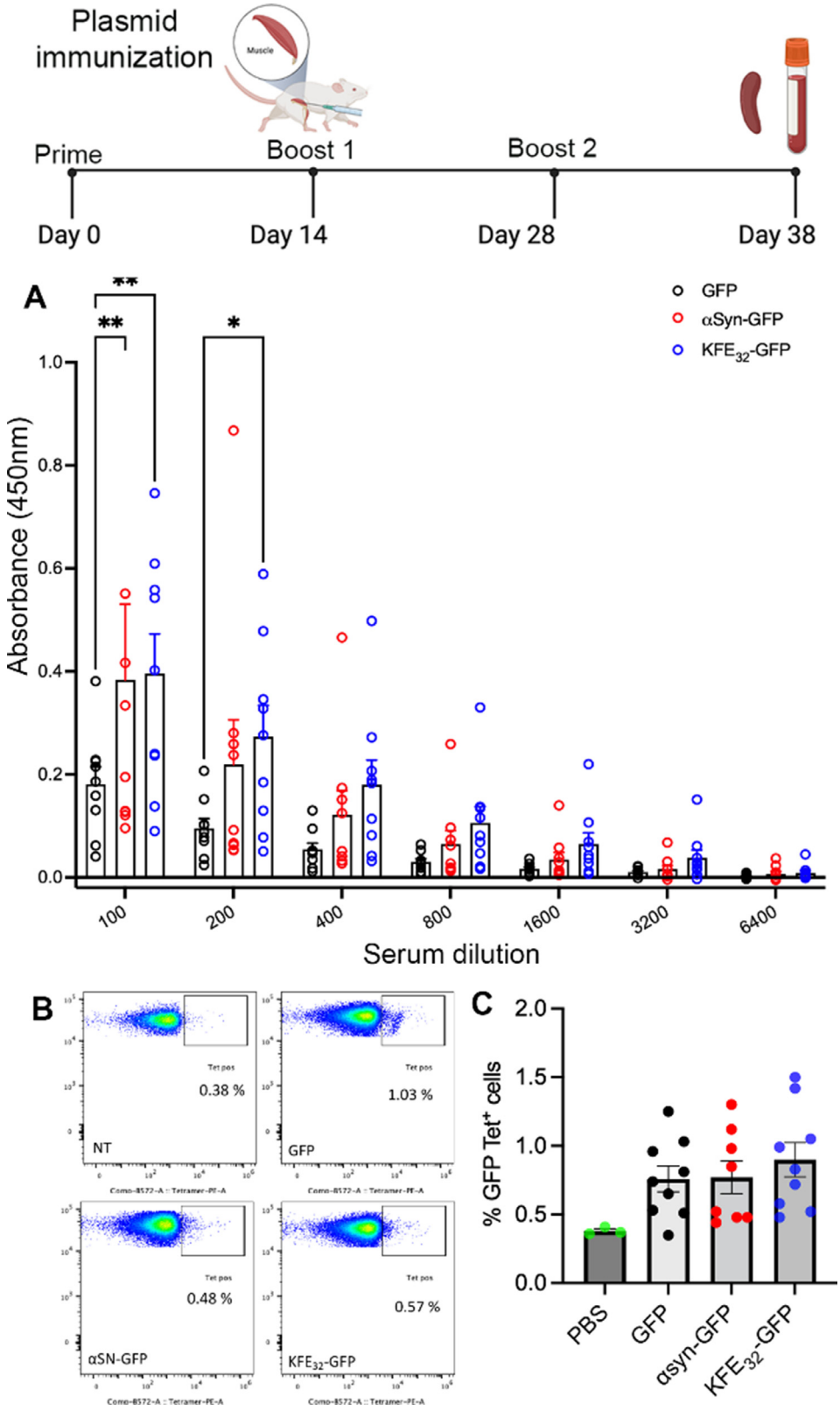

Fig. 5. DNA vaccination with KFE_{32}-GFP constructs elicits robust immune responses. (A) Prime-boost with KFE_{32}-GFP construct induced robust anti-GFP (total IgG H±L) antibody responses at significantly higher levels compared to α-syn-GFP or soluble GFP at higher serum dilutions. Levels of total IgG were comparable between α-syn-GFP fusion or soluble GFP. $^{*}p \leq 0.05$ and $^{**}p \leq 0.01$ by ANOVA with Tukey HSD post hoc testing, compared between groups. (B) Representative flow cytometry plots showing production of tetramer$^{\pm}$ CD8$^{\pm}$ T cells in the spleens of mice immunized with soluble GFP, α-syn-GFP, or KFE_{32}-GFP. (C) Cumulative bar graph from (B) showing the percentage of tetramer$^{\pm}$ CD8$^{\pm}$ T cells from two independent plasmid batches and two independent animal experiments (n = 4-5 mice per group). Vaccination scheme was created using Biorender.com

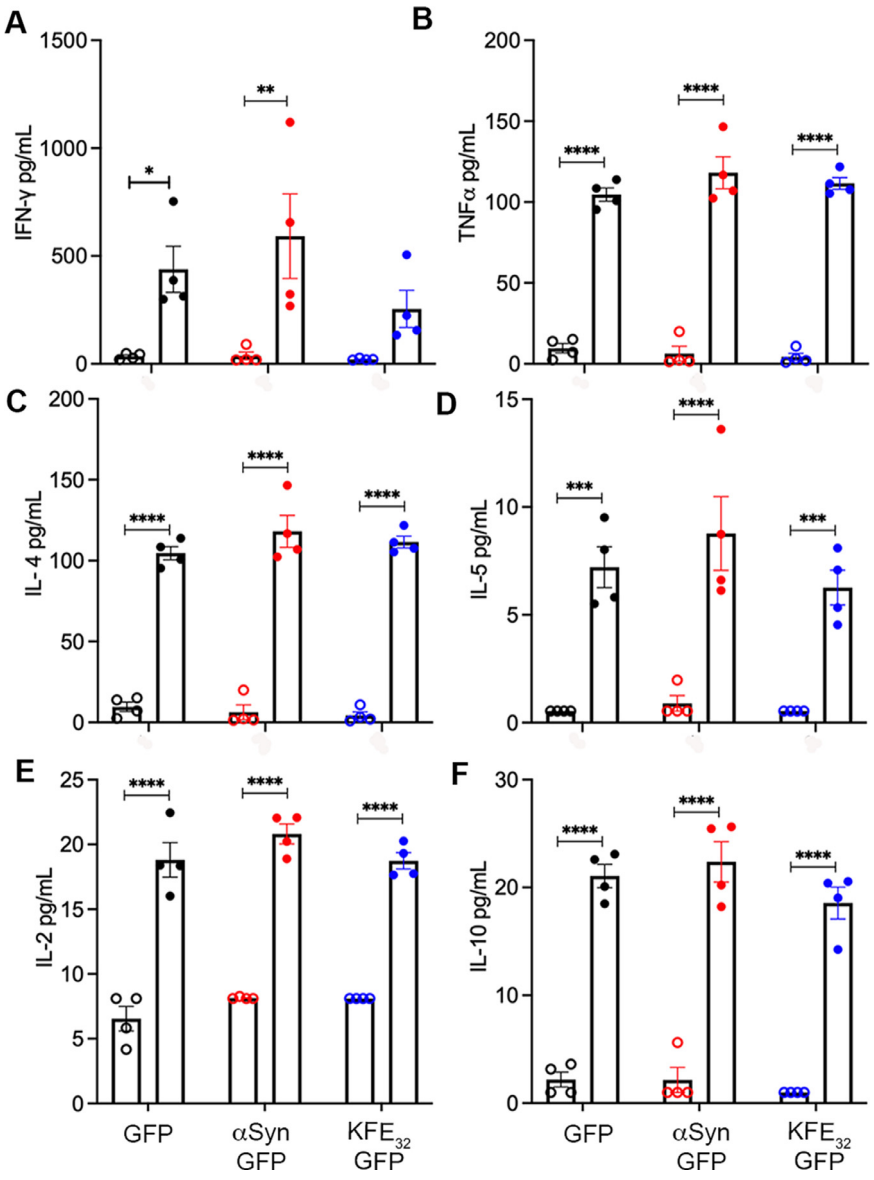

Fig. 6. DNA vaccination with KFE_{32}-GFP elicits a balanced Th1/Th2 response. (A) Production of Th1 cytokines (A) IFN-γ, (B) TNF-α (E) IL-2 and Th2 cytokines (C) IL-4 (D) IL-5 and (F) IL-10 in unstimulated (open circle) or stimulated (solid circle) splenocyte cultures from mice vaccinated with soluble GFP, αSyn-GFP, or KFE_{32}-GFP constructs. $^{*}p < 0.05$, $^{**}p < 0.01$, $^{***}p < 0.001$, $^{****}p < 0.0001$ compared with corresponding unchallenged control, by ANOVA with Sidak's multiple comparisons test.

generation of adjuvants including MF59 are under development [56]. These adjuvants are chemically heterogeneous mixtures of plant- or pathogen-derived products, formulations of mineral salts, or emulsions, all of which which suffer from poor chemical definition. These limitations have motivated the pursuit of adjuvant-free vaccination technologies [57]. Recently, Matrix M, a nanoparticle-based adjuvant platform licensed by Novavax has been FDA approved for use in COVID-19 vaccines [55] paving the way for the next generation of nano-adjuvants.

To enhance vaccine-based immunotherapies to combat infections, cancer, and other conditions, biomaterials are being heavily explored with the goal of improving vaccine safety and efficacy. A prominent strategy, inspired by viruses, is to leverage macromolecular self-assembly which facilitates multivalent antigen display, significantly enhancing receptor binding affinity and immunogenicity. Recently, peptides that self-assemble into specific nanoarchitectures have been pursued as modular and chemically defined platforms for vaccine development [4]. In particular, 'amyloid-inspired' peptide nanofibers that adopt a cross-β structure have been demonstrated to be effective for efficient delivery of vaccines and immunotherapies in multiple preclinical models of infectious and non-infectious diseases [4]. However, several unresolved challenges still remain and must be addressed to accelerate translational efforts. A key hurdle is the fact that the safety of using cross-β sheet rich amyloid-like structures must be carefully studied [4].

The field of peptide self-assembly was motivated by initial attempts to gain molecular and structural information on misfolded states of proteins involved in neurodegenerative diseases. Identification of minimal peptide fragments capable of emulating the behavior of the parent protein was used as a reductionist approach to glean structural information and understand disease pathogenesis. Unexpectedly, these studies also suggested that very small peptides are capable of self-assembly. Minimal sequences derived from natural proteins such as islet amyloid polypeptide (FGAILK), human calcitonin (DNFKFA), and $A\beta_{1\text{-}42}$ (KLVFFA) have been reported [58–62]. Reches and Gazit first identified the diphenylalanine (FF) peptide as the shortest motif able to self-assemble from the full length

amyloid beta peptide ($A\beta_{1\text{-}42}$) [63]. A second family of cross-β rich peptides comprised of amphipathic sequences with strictly alternating apolar and charged residues, such as the protopeptide EAK [Ac-$(AEAEAKAK)_2$-NH_2], were first identified in *S. cerevisiae* [64]. Because these peptides all self assemble into structures resembling amyloid fibrils, and amyloid underpins the pathogenesis of several neurodegenerative diseases, understanding the amyloidogenic potential of cross-β rich peptide biomaterials intended for vaccine development or other *in vivo* applications is paramount for their continued success. Computational and spectroscopic efforts in structural biology have identified that cross-β rich peptide aggregates are characterized by remarkable molecular and structural complexities that correlate with toxicity [65]. Importantly, the outcomes of these studies have been exploited to design peptide inhibitors of amyloid-aggregation and cross-β rich peptide fibrils have also been reported to be capable of triggering innate immune pathways for the design of vaccines [8,65–67]. Also, emerging insights into the functional roles of amyloid and amyloid-like proteins have challenged the notion that all amyloid species are inherently toxic, and crucial differences that distinguish pathological, inconsequential, and functional aggregation are not yet fully understood.

In this study we utilized the self-assembling peptide KFE_8 (FKFEFKFE). This peptide sequence is not only Phe rich but also amphipathic with alternating apolar and charged residues. Association of the two apolar faces generates the basic cross-β motif that constitutes the backbone of the fibrils. The structure, molecular packing, and assembly of KFE_8 have been extensively characterized using spectroscopic and computational studies [7,18,19]. Further, we have demonstrated the ability of KFE_8 to act as an immune adjuvant in multiple preclinical models of disease [4]. Therefore, we anticipate that, barring safety concerns, the KFE_8 sequence may have broad translational utility. Here, to further the translational potential of amyloid-inspired peptide nanofibers, we have investigated the properties of the self-assembling peptide KFE_8. First, we leveraged the genetic tractability of *S. cerevisiae*, Baker's yeast, to characterize varying lengths of this repeat. We find that KFE_8 repeats have distinct properties from those of amyloid and amyloid-like proteins. While KFE_8 forms characteristic insoluble inclusions, expression of these materials is non-toxic. We have previously reported that KFE_8 fibrils can enter cells via endocytic mechanisms, and that the adjuvanting potential of peptide nanofibers is due to their ability to engage key components of the autophagy pathway [47]. Triggering autophagy is important, because this significantly improves responses to influenza vaccines in the elderly and the BCG vaccine in infants [68]. However, amyloid species are also cleared via autophagy, and evidence suggests that impairment of autophagy in the elderly may be linked to increased susceptibility to neurodegeneration with aging [69]. Here, we find that just as these peptides are cleared via autophagy in mammalian cells, they are also cleared via autophagy in yeast. Promisingly, even in an autophagy-impaired strain, expression of the KFE_8 sequences remains non-toxic in yeast. The ability to study these biomaterials upon expression in yeast will be a useful platform in further characterization of these materials. For instance, this yeast expression platform can be used to conduct a genome-wide screen to investigate if the KFE repeat peptides engage or interact with other proteins in the cell, and to investigate and/or identify possible off-target effects.

Accumulating evidence implicates transcellular propagation of amyloid species, or seeds, as a mechanism for disease progression in neurodegeneration. Amyloid species are also known to be capable of 'cross-seeding', whereby amyloid fibrils comprised of one protein can initiate the amyloid cascade of another amyloidogenic protein. This is thought to be due to the highly conserved structural features of amyloid and pre-amyloid, which are highlighted by the findings that a single antibody can cross-react with pre-amyloid species comprised of a diverse range of monomeric proteins [14]. As such, it is crucial to investigate the capacity of any amyloid-like therapeutics to seed amyloidogenesis of endogenous proteins. Here, we find that while α-syn preformed fibrils can enter the cell and trigger robust seeding of endogenous α-syn, KFE_8 fibrils can also enter the cell, but they do not trigger seeding of α-syn amyloidogenesis. In future work it will be important to confirm that these fibrils do not cross-seed a broader range of amyloidogenic proteins.

Finally, inspired by our successful expression of the KFE-GFP fusions in yeast, we also explored the development of DNA-based vaccines using the KFE platform. DNA-based vaccines remain an infrequently employed mode of delivery, yet this strategy has great promise. By genetically encoding synthesis of a vaccine, longer sequences can be made than is practical by synthetic routes. Further, DNA is less expensive to generate, easier to modify, and can be stored at ambient temperatures. To investigate these applications, we immunized mice with plasmids encoding KFE_{32}-GFP, where GFP serves as a model antigen. Immunization elicited a robust immune response, and the KFE_{32} scaffold induced production of significantly higher levels of anti-GFP antibodies as compared to immunization with plasmid encoding GFP alone. However, a key observation here is that the antibody levels were low compared to other reports using peptide nanofibers vaccines. To date, a plasmid vaccine encoding peptide nanofibers has not been tested so we do not have a comparative baseline. Hudalla et al. delivered GFP conjugated to peptide nanofibers (via cutinase-phosphonate orthogonal chemistry) and reported high anti-GFP antibody titers [70]. On the contrary, immunization with GFP tagged PolyQ repeats (103Q) delivered as a plasmid, produced low levels of anti-GFP antibodies as observed here for KFE_{32}-GFP repeats. Importantly, the self-adjuvanting potential observed upon immunization with synthetic peptide nanofibers was not diminished when delivered for expression from a DNA plasmid. Further, the cytokine profiles from antigen recall assays indicate a balanced Th1/Th2 response.

In summary, we demonstrate that expression of KFE_8 results in the formation of insoluble inclusions in yeast similar to those of amyloid and amyloid-like proteins. However, KFE_8 is not toxic and toxicity is not exacerbated in autophagy-deficient yeast. Further, synthetic KFE_8 nanofibers do not cross-seed the amyloidogenesis of α-synuclein, even at 1000× higher concentrations compared to α-syn preformed fibrils. In mice, vaccination with plasmids encoding KFE_{32}-GFP elicited a robust cellular immune response with a balanced Th1/Th2 cytokine profile, along with generation of antigen-specific $CD8^+$T cells. These findings are significant and exciting because, since their serendipitous discovery, several applications based on self-assembling peptide nanofibers have been brought to the market and new sequences are being designed to generate chemically defined and hierarchically organized nanoscale materials. However, to date no studies have investigated the amyloidogenic potential of self-assembling peptides or their utility as DNA vaccines. Our results demonstrate that despite their molecular, structural, and morphological similarity to pathological amyloids, self-assembling peptides have distinct properties, and are promising materials for biomedical applications.

Data availibility

Data will be made available on request.

Declaration of Competing Interest

The authors declare that they have no known competing financial interests or personal relationships that could have appeared to influence the work reported in this paper.

Acknowledgments

This study was supported by NIH grant R21AG068733 (to J.S.R. and M.E.J.) and National Science Foundation CAREER award to J.S.R. The authors acknowledge financial support from Washington University in St. Louis and the Institute of Materials Science and Engineering for the use of instruments and staff assistance.

Supplementary materials

Supplementary material associated with this article can be found, in the online version, at doi:10.1016/j.actbio.2023.08.015.

References

[1] J. Li, R. Xing, S. Bai, X. Yan, Recent advances of self-assembling peptide-based hydrogels for biomedical applications, Soft Matter 15 (8) (2019) 1704–1715.
[2] C. Zhao, H. Chen, F. Wang, X. Zhang, Amphiphilic self-assembly peptides: rational strategies to design and delivery for drugs in biomedical applications, Colloids Surf. B Biointerfaces 208 (2021) 112040.
[3] Y. Wen, J.H. Collier, Supramolecular peptide vaccines: tuning adaptive immunity, Curr. Opin. Immunol. 35 (2015) 73–79.
[4] C.L. O'Neill, P.C. Shrimali, Z.P. Clapacs, M.A. Files, J.S. Rudra, Peptide-based supramolecular vaccine systems, Acta Biomater. 133 (2021) 153–167.
[5] H. Acar, S. Srivastava, E.J. Chung, M.R. Schnorenberg, J.C. Barrett, J.L. LaBelle, M. Tirrell, Self-assembling peptide-based building blocks in medical applications, Adv Drug Deliv. Rev. 110-111 (2017) 65–79.
[6] N.J. Sinha, M.G. Langenstein, D.J. Pochan, C.J. Kloxin, J.G. Saven, Peptide design and self- assembly into targeted nanostructure and functional materials, Chem. Rev. 121 (22) (2021) 13915–13935.
[7] C.J. Bowerman, B.L. Nilsson, Self-assembly of amphipathic beta-sheet peptides: insights and applications, Biopolymers 98 (3) (2012) 169–184.
[8] N. Balasco, C. Diaferia, G. Morelli, L. Vitagliano, A. Accardo, Amyloid-like aggregation in diseases and biomaterials: osmosis of structural information, Front. Bioeng. Biotechnol. 9 (2021) 641372.
[9] C.M. Dobson, Protein folding and misfolding, Nature 426 (6968) (2003) 884–890.
[10] R.I. Morimoto, Stress, aging, and neurodegenerative disease, N. Engl. J. Med. 355 (21) (2006) 2254–2255.
[11] M.L. Sprunger, M.E. Jackrel, Prion-like proteins in phase separation and their link to disease, Biomolecules 11 (7) (2021) 1014.
[12] C. Rapezzi, C.C. Quarta, L. Riva, S. Longhi, I. Gallelli, M. Lorenzini, P. Ciliberti, E. Biagini, F. Salvi, A. Branzi, Transthyretin-related amyloidoses and the heart: a clinical overview, Nat. Rev. Cardiol. 7 (7) (2010) 398–408.
[13] M. Ankarcrona, B. Winblad, C. Monteiro, C. Fearns, E.T. Powers, J. Johansson, G.T. Westermark, J. Presto, B.G. Ericzon, J.W. Kelly, Current and future treatment of amyloid diseases, J. Intern. Med. 280 (2) (2016) 177–202.
[14] R. Kayed, E. Head, J.L. Thompson, T.M. McIntire, S.C. Milton, C.W. Cotman, C.G. Glabe, Common structure of soluble amyloid oligomers implies common mechanism of pathogenesis, Science 300 (5618) (2003) 486–489.
[15] B. Ren, Y. Zhang, M. Zhang, Y. Liu, D. Zhang, X. Gong, Z. Feng, J. Tang, Y. Chang, J. Zheng, Fundamentals of cross-seeding of amyloid proteins: an introduction, J. Mater. Chem. B 7 (46) (2019) 7267–7282.
[16] J. Vaneyck, I. Segers-Nolten, K. Broersen, M. Claessens, Cross-seeding of alpha-synuclein aggregation by amyloid fibrils of food proteins, J. Biol. Chem. 296 (2021) 100358.
[17] T. Abudula, K. Bhatt, L.J. Eggermont, N. O'Hare, A. Memic, S.A. Bencherif, Supramolecular self-assembled peptide-based vaccines: current state and future perspectives, Front. Chem. 8 (2020) 598160.
[18] C.J. Bowerman, D.M. Ryan, D.A. Nissan, B.L. Nilsson, The effect of increasing hydrophobicity on the self-assembly of amphipathic beta-sheet peptides, Mol. Biosyst. 5 (9) (2009) 1058–1069.
[19] N.R. Lee, C.J. Bowerman, B.L. Nilsson, Sequence length determinants for self--assembly of amphipathic beta-sheet peptides, Biopolymers 100 (6) (2013) 738–750.
[20] R.J. Swanekamp, J.T. DiMaio, C.J. Bowerman, B.L. Nilsson, Coassembly of enantiomeric amphipathic peptides into amyloid-inspired rippled beta-sheet fibrils, J. Am. Chem. Soc. 134 (12) (2012) 5556–5559.
[21] T.M. Clover, C.L. O'Neill, R. Appavu, G. Lokhande, A.K. Gaharwar, A.E. Posey, M.A. White, J.S. Rudra, Self-assembly of block heterochiral peptides into helical tapes, J. Am. Chem. Soc. 142 (47) (2020) 19809–19813.
[22] R. Appavu, C.B. Chesson, A.Y. Koyfman, J.D. Snook, F.J. Kohlhapp, A. Zloza, J.S. Rudra, Enhancing the magnitude of antibody responses through biomaterial stereochemistry, Acs Biomater.-Sci. Eng. 1 (7) (2015) 601–609.
[23] C.B. Chesson, M. Huante, R.J. Nusbaum, A.G. Walker, T.M. Clover, J. Chinnaswamy, J.J. Endsley, J.S. Rudra, Nanoscale peptide self-assemblies boost BCG-primed cellular immunity against mycobacterium tuberculosis, Sci. Rep. 8 (1) (2018) 12519.
[24] B.M. Friedrich, D.W. Beasley, J.S. Rudra, Supramolecular peptide hydrogel adjuvanted subunit vaccine elicits protective antibody responses against West Nile virus, Vaccine 34 (46) (2016) 5479–5482.
[25] J.S. Rudra, Y. Ding, H. Neelakantan, C. Ding, R. Appavu, S. Stutz, J.D. Snook, H. Chen, K.A. Cunningham, J. Zhou, Suppression of cocaine-evoked hyperactivity by self- adjuvanting and multivalent peptide nanofiber vaccines, ACS Chem. Neurosci. 7 (5) (2016) 546–552.
[26] J.P. Taylor, R.H. Brown Jr., D.W. Cleveland, Decoding ALS: from genes to mechanism, Nature 539 (7628) (2016) 197–206.
[27] B.B. Holmes, M.I. Diamond, Cellular models for the study of prions, Cold Spring Harbor Perspect. Med. 7 (2) (2017).
[28] B.B. Holmes, J.L. Furman, T.E. Mahan, T.R. Yamasaki, H. Mirbaha, W.C. Eades, L. Belaygorod, N.J. Cairns, D.M. Holtzman, M.I. Diamond, Proteopathic tau seeding predicts tauopathy *in vivo*, Proc. Natl. Acad. Sci. USA 111 (41) (2014) E4376–E4385.
[29] E.A. Winzeler, D.D. Shoemaker, A. Astromoff, H. Liang, K. Anderson, B. Andre, R. Bangham, R. Benito, J.D. Boeke, H. Bussey, A.M. Chu, C. Connelly, K. Davis, F. Dietrich, S.W. Dow, M. El Bakkoury, F. Foury, S.H. Friend, E. Gentalen, G. Giaever, J.H. Hegemann, T. Jones, M. Laub, H. Liao, N. Liebundguth, D.J. Lockhart, A. Lucau- Danila, M. Lussier, N. M'Rabet, P. Menard, M. Mittmann, C. Pai, C. Rebischung, J.L. Revuelta, L. Riles, C.J. Roberts, P. Ross-MacDonald, B. Scherens, M. Snyder, S. Sookhai-Mahadeo, R.K. Storms, S. Véronneau, M. Voet, G. Volckaert, T.R. Ward, R. Wysocki, G.S. Yen, K. Yu, K. Zimmermann, P. Philippsen, M. Johnston, R.W. Davis, Functional characterization of the S. cerevisiae genome by gene deletion and parallel analysis, Science 285 (5429) (1999) 901–906.
[30] S. Alberti, A.D. Gitler, S. Lindquist, A suite of gateway cloning vectors for high-throughput genetic analysis in *Saccharomyces cerevisiae*, Yeast 24 (10) (2007) 913–919.
[31] M.E. Jackrel, M.E. DeSantis, B.A. Martinez, L.M. Castellano, R.M. Stewart, K.A. Caldwell, G.A. Caldwell, J. Shorter, Potentiated Hsp104 variants antagonize diverse proteotoxic misfolding events, Cell 156 (1–2) (2014) 170–182.
[32] R.D. Gietz, R.H. Schiestl, High-efficiency yeast transformation using the LiAc/SS carrier DNA/PEG method, Nat. Protoc. 2 (1) (2007) 31–34.
[33] J.C. Kessler, J.C. Rochet, P.T. Lansbury Jr., The N-terminal repeat domain of alpha- synuclein inhibits beta-sheet and amyloid fibril formation, Biochemistry 42 (3) (2003) 672–678.
[34] J. Choi, M.L. Cooper, B. Alahmari, J. Ritchey, L. Collins, M. Holt, J.F. DiPersio, Pharmacologic blockade of JAK1/JAK2 reduces GvHD and preserves the graft-versus- leukemia effect, PLoS One 9 (10) (2014) e109799.
[35] E. Campeau, V.E. Ruhl, F. Rodier, C.L. Smith, B.L. Rahmberg, J.O. Fuss, J. Campisi, P. Yaswen, P.K. Cooper, P.D. Kaufman, A versatile viral system for expression and depletion of proteins in mammalian cells, PLoS One 4 (8) (2009) e6529.
[36] T. Dull, R. Zufferey, M. Kelly, R.J. Mandel, M. Nguyen, D. Trono, L. Naldini, A third- generation lentivirus vector with a conditional packaging system, J. Virol. 72 (11) (1998) 8463–8471.
[37] V. Khurana, S. Lindquist, Modelling neurodegeneration in *Saccharomyces cerevisiae*: why cook with baker's yeast? Nat. Rev. Neurosci. 11 (6) (2010) 436–449.
[38] A.C. Elden, H.J. Kim, M.P. Hart, A.S. Chen-Plotkin, B.S. Johnson, X. Fang, M. Armakola, F. Geser, R. Greene, M.M. Lu, A. Padmanabhan, D. Clay-Falcone, L. McCluskey, L. Elman, D. Juhr, P.J. Gruber, U. Rub, G. Auburger, J.Q. Trojanowski, V.M. Lee, V.M. Van Deerlin, N.M. Bonini, A.D. Gitler, Ataxin-2 intermediate-length polyglutamine expansions are associated with increased risk for ALS, Nature 466 (7310) (2010) 1069- 75.
[39] Z. Sun, Z. Diaz, X. Fang, M.P. Hart, A. Chesi, J. Shorter, A.D. Gitler, Molecular determinants and genetic modifiers of aggregation and toxicity for the ALS disease protein FUS/TLS, PLoS Biol. 9 (4) (2011) e1000614.
[40] S. Ju, D.F. Tardiff, H. Han, K. Divya, Q. Zhong, L.E. Maquat, D.A. Bosco, L.J. Hayward, R.H. Brown Jr., S. Lindquist, D. Ringe, G.A. Petsko, A yeast model of FUS/TLS- dependent cytotoxicity, PLoS Biol. 9 (4) (2011) e1001052.
[41] S. Treusch, S. Hamamichi, J.L. Goodman, K.E.S. Matlack, C.Y. Chung, V. Baru, J.M. Shulman, A. Parrado, B.J. Bevis, J.S. Valastyan, H. Han, M. Lindhagen-Persson, E.M. Reiman, D.A. Evans, D.A. Bennett, A. Olofsson, P.L. DeJager, R.E. Tanzi, K.A. Caldwell, G.A. Caldwell, S. Lindquist, Functional links between Aβ toxicity, endocytic trafficking, and Alzheimer's disease risk factors in yeast, Science 334 (6060) (2011) 1241–1245.
[42] T.F. Outeiro, S. Lindquist, Yeast cells provide insight into alpha-synuclein biology and pathobiology, Science 302 (5651) (2003) 1772–1775.
[43] J.J. Ryan, M.L. Sprunger, K. Holthaus, J. Shorter, M.E. Jackrel, Engineered protein disaggregases mitigate toxicity of aberrant prion-like fusion proteins underlying sarcoma, J. Biol. Chem. 294 (29) (2019) 11286–11296.
[44] C. Kayatekin, A. Amasino, G. Gaglia, J. Flannick, J.M. Bonner, S. Fanning, P. Narayan, M.I. Barrasa, D. Pincus, D. Landgraf, J. Nelson, W.R. Hesse, M. Costanzo, C.L. Myers, C. Boone, J.C. Florez, S. Lindquist, Translocon declogger Ste24 protects against IAPP oligomer-induced proteotoxicity, Cell 173 (1) (2018) 62–73 e9.
[45] M.L. Sprunger, K. Lee, B.S. Sohn, M.E. Jackrel, Molecular determinants and modifiers of Matrin-3 toxicity, condensate dynamics, and droplet morphology, iScience 25 (3) (2022).
[46] B.S. Johnson, J.M. McCaffery, S. Lindquist, A.D. Gitler, A yeast TDP-43 proteinopathy model: exploring the molecular determinants of TDP-43 aggregation and cellular toxicity, Proc. Natl. Acad. Sci. USA 105 (17) (2008) 6439–6444.
[47] J.S. Rudra, A. Khan, T.M. Clover, J.J. Endsley, A. Zloza, J. Wang, C. Jagannath, Supramolecular peptide nanofibers engage mechanisms of autophagy in antigen- presenting cells, ACS Omega 2 (12) (2017) 9136–9143.
[48] S. Alberti, R. Halfmann, S. Lindquist, Biochemical, cell biological, and genetic assays to analyze amyloid and prion aggregation in yeast, Methods Enzymol. 470 (2010) 709–734.

[49] L. Sun, X. Zhao, A self-assembling peptide RADA16-I integrated with spider fibroin uncrystalline motifs, Int. J. Nanomed. 7 (2012) 571–580.
[50] K.C. Luk, V. Kehm, J. Carroll, B. Zhang, P. O'Brien, J.Q. Trojanowski, V.M.Y. Lee, Pathological α-synuclein transmission initiates parkinson-like neurodegeneration in nontransgenic mice, Science 338 (6109) (2012) 949–953.
[51] X. Zottig, S. Al-Halifa, M. Côté-Cyr, C. Calzas, R. Le Goffic, C. Chevalier, D. Archambault, S. Bourgault, Self-assembled peptide nanorod vaccine confers protection against influenza a virus, Biomaterials 269 (2021) 120672.
[52] P.O. Ilyinskii, G. Thoidis, M.Y. Sherman, A. Shneider, Adjuvant potential of aggregate- forming polyglutamine domains, Vaccine 26 (26) (2008) 3223–3226.
[53] T. Olafsdottir, M. Lindqvist, A.M. Harandi, Molecular signatures of vaccine adjuvants, Vaccine 33 (40) (2015) 5302–5307.
[54] M.L. Mbow, E. De Gregorio, N.M. Valiante, R. Rappuoli, New adjuvants for human vaccines, Curr. Opin. Immunol. 22 (3) (2010) 411–416.
[55] B. Pulendran, P.S. Arunachalam, D.T. O'Hagan, Emerging concepts in the science of vaccine adjuvants, Nat. Rev. Drug Discov. 20 (6) (2021) 454–475.
[56] S. Kommareddy, M. Singh, D.T. O'Hagan, Chapter 13 - MF59: a safe and potent adjuvant for human use, in: V.E.J.C. Schijns, D.T. O'Hagan (Eds.), Immunopotentiators in Modern Vaccines, Second Edition, Academic Press, 2017, pp. 249–263.
[57] A.N. Tsoras, J.A. Champion, Protein and peptide biomaterials for engineered subunit vaccines and immunotherapeutic applications, Annu. Rev. Chem. Biomol. Eng. 10 (10) (2019) 337–359.
[58] K. Tenidis, M. Waldner, J. Bernhagen, W. Fischle, M. Bergmann, M. Weber, M.L. Merkle, W. Voelter, H. Brunner, A. Kapurniotu, Identification of a penta- and hexapeptide of islet amyloid polypeptide (IAPP) with amyloidogenic and cytotoxic properties, J. Mol. Biol. 295 (4) (2000) 1055–1071.
[59] A. Kazantzis, M. Waldner, J.W. Taylor, A. Kapurniotu, Conformationally constrained human calcitonin (hCt) analogues reveal a critical role of sequence 17-21 for the oligomerization state and bioactivity of hCt, Eur. J. Biochem. 269 (3) (2002) 780–791.
[60] C. Hilbich, B. Kisters-Woike, J. Reed, C.L. Masters, K. Beyreuther, Substitutions of hydrophobic amino acids reduce the amyloidogenicity of Alzheimer's disease beta A4 peptides, J. Mol. Biol. 228 (2) (1992) 460–473.
[61] S. Zhang, T. Holmes, C. Lockshin, A. Rich, Spontaneous assembly of a self-complementary oligopeptide to form a stable macroscopic membrane, Proc. Natl. Acad. Sci. U.S.A. 90 (8) (1993) 3334–3338.
[62] X. Zhao, S. Zhang, Fabrication of molecular materials using peptide construction motifs, Trends Biotechnol. 22 (9) (2004) 470–476.
[63] M. Reches, E. Gazit, Casting metal nanowires within discrete self-assembled peptide nanotubes, Science 300 (5619) (2003) 625–627.
[64] S. Zhang, C. Lockshin, A. Herbert, E. Winter, A. Rich, Zuotin, a putative Z-DNA binding protein in *Saccharomyces cerevisiae*, EMBO J. 11 (10) (1992) 3787–3796.
[65] J. Nasica-Labouze, P.H. Nguyen, F. Sterpone, O. Berthoumieu, N.V. Buchete, S. Cote, A. De Simone, A.J. Doig, P. Faller, A. Garcia, A. Laio, M.S. Li, S. Melchionna, N. Mousseau, Y. Mu, A. Paravastu, S. Pasquali, D.J. Rosenman, B. Strodel, B. Tarus, J.H. Viles, T. Zhang, C. Wang, P. Derreumaux, Amyloid beta protein and Alzheimer's disease: when computer simulations complement experimental studies, Chem. Rev. 115 (9) (2015) 3518–3563.
[66] S.L. Griner, P. Seidler, J. Bowler, K.A. Murray, T.P. Yang, S. Sahay, M.R. Sawaya, D. Cascio, J.A. Rodriguez, S. Philipp, J. Sosna, C.G. Glabe, T. Gonen, D.S. Eisenberg, Structure-based inhibitors of amyloid beta core suggest a common interface with tau, eLife 8 (2019).
[67] S. Al-Halifa, X. Zottig, M. Babych, M. Cote-Cyr, S. Bourgault, D. Archambault, Harnessing the activation of toll-like receptor 2/6 by self-assembled cross–beta fibrils to design adjuvanted nanovaccines, Nanomaterials (Basel) 10 (10) (2020).
[68] C. Jagannath, D.R. Lindsey, S. Dhandayuthapani, Y. Xu, R.L. Hunter Jr., N.T. Eissa, Autophagy enhances the efficacy of BCG vaccine by increasing peptide presentation in mouse dendritic cells, Nat. Med. 15 (3) (2009) 267–276.
[69] S. Giovedi, M.M. Ravanelli, B. Parisi, B. Bettegazzi, F.C. Guarnieri, Dysfunctional autophagy and endolysosomal system in neurodegenerative diseases: relevance and therapeutic options, Front. Cell Neurosci. 14 (2020) 602116.
[70] G.A. Hudalla, J.A. Modica, Y.F. Tian, J.S. Rudra, A.S. Chong, T. Sun, M. Mrksich, J.H. Collier, A self-adjuvanting supramolecular vaccine carrying a folded protein antigen, Adv. Healthc. Mater. 2 (8) (2013) 1114–1119.